Talanta 207 (2020) 120341

Contents lists available at ScienceDirect

Talanta

journal homepage: www.elsevier.com/locate/talanta

Sodium hexametaphosphate modulated fluorescence responsive biosensor based on self-assembly / disassembly mode of reduced-graphene quantum dots / chitosan system for alkaline phosphatase

Fanping Shi[a,b], Jiao Li[c], Jingjing Sun[a], Hui Huang[c], Xingguang Su[b,**], Zonghua Wang[a,*]

[a] Shandong Sino-Japanese Center for Collaborative Research of Carbon Nanomaterials, College of Chemistry and Chemical Engineering, Qingdao University, Qingdao, Shandong, 266071, PR China
[b] Department of Analytical Chemistry, College of Chemistry, Jilin University, 2699 Qianjin Street, Changchun, 130012, China
[c] College of Food Science and Engineering, Jilin University, Changchun, 130025, China

ARTICLE INFO

Keywords:
Graphene quantum dots
Alkaline phosphatase
Chitosan
Fluorescent detection
Self-assembly

ABSTRACT

Herein, a sodium hexametaphosphate ($(NaPO_3)_6$) modulated fluorescence responsive probe based on the integration of reduced graphene quantum dots (rGQDs) and chitosan (CS) via self-assembly/disassembly for label-free alkaline phosphatase assay was constructed. The cationic-charged CS can couple with anionic rGQDs and quench their fluorescence intensity through electrostatic attraction and structure transformation. This self-assembly system above could be decomposed when $(NaPO_3)_6$ present, because $(NaPO_3)_6$ could competes with rGQDs for the binding sites on the CS, leading to the disassembly of the rGQDs/CS system, as well as to the system exhibiting a turn-on fluorescence signal. By introducing alkaline phosphatase (ALP) into the system, $(NaPO_3)_6$ can be hydrolyzed to give phosphate anions. The decomposition effect of enzymatic products on the rGQDs/CS system is weakened. Thus the self-assembling system shows a decreasing photoluminescence (PL) signal compared with the rGQDs/CS-$(NaPO_3)_6$ disassembling system. The concentration of ALP can be reflected by the variation of the PL intensity of rGQDs/CS system mixed with the enzymatic hydrolysis products. The dynamic detection range for ALP is 20–500 mU mL^{-1}, with a detection limit (LOD) of 7.8 mU mL^{-1}. The present fluorescence probe based on the rGQDs/CS system for ALP has excellent selectivity and strong anti-interference capability. When applied to real samples analysis, the present strategy exhibits satisfactory results. In addition, the rGQDs/CS system was used to fabricate paper-based test strips for visual detection of ALP activity, validating its great potential in the application of on-site ALP assays.

1. Introduction

Alkaline phosphatase (ALP) belongs to the group of hydrolases that are located primarily in human liver and other human organisms [1]. The main function of ALP is to dephosphorylate various monophosphate esters substrates into inorganic phosphates [2] such as adenosine triphosphate (ATP), ascorbic acid-2-phosphate (AAP) and *p*-nitrophenyl phosphate (pNPP). The abnormal levels of ALP in serum are regarded as an important diagnostic indicator for physiologic or pathologic changes such as hepatic disease (hepatitis and liver dysfunction), bone disease (osteoporosis, osteomalacia and bone tumor), and ovarian and breast cancer [3–5]. Therefore, serum ALP determination is frequently a part of routine blood tests and has clinical implications [6]. Fluorescence assays are usually chosen preferentially for ALP determination due to their sensitivity and simplicity. Currently, the fluorescence biosensors designed for ALP determination can be divided into three categories according to the detection mechanism: 1) the hydrolysate of ALP can separate the fluorescent probes and the quenching agents, interrupting the energy transfer or electron transfer process between the two; alternatively, the hydrolysate quenches the fluorescence probes directly, leading to a change in the photoluminescence (PL) signal. This sensing-mode is commonly observed in the “turn-off-on” and “turn-off” sensing assay [7–13]; 2) the substrate of ALP can enhance the PL intensity of the probes, but the hydrolysis process disintegrates the probes, resulting in a decreased PL signal. This mode is commonly observed in the biosensors based on the ATP template-synthesized metal clusters [14]; 3) the electronegativity of the probe or the entire fluorescence detection system changed because ALP hydrolyzes the phosphate group at the

* Corresponding author.
** Corresponding author.
E-mail addresses: suxg@jlu.edu.cn (X. Su), wangzonghua@qdu.edu.cn (Z. Wang).

https://doi.org/10.1016/j.talanta.2019.120341
Received 24 May 2019; Received in revised form 3 September 2019; Accepted 7 September 2019
Available online 12 September 2019
0039-9140/

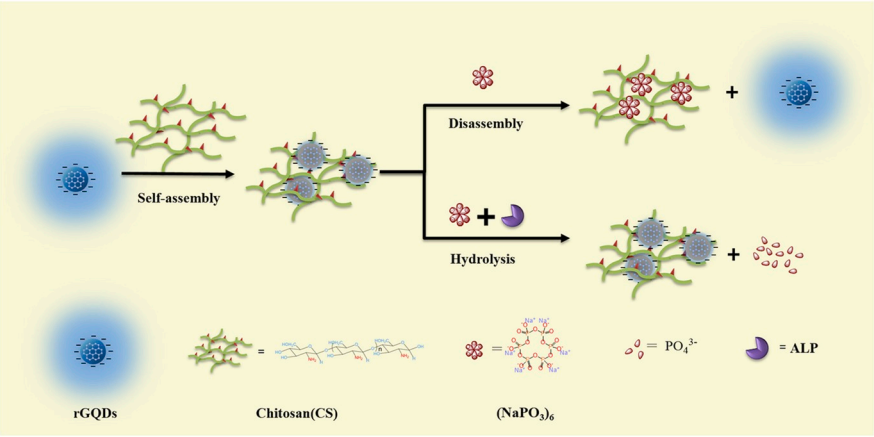

Scheme 1. The schematic illustration of fluorescent assay for monitoring ALP activity based on the self-assembly of chitosan and rGQDs.

edge of the fluorescence probes or the phosphates released into the solution by the enzymatic hydrolysis of ALP, causing the fluorescence intensity of the probe changes due to aggregation or sedimentation. This sensing-mode is commonly occurred in the biosensors based on aggregation-induced-emission (AIE) materials [15–17]. While these sensing platforms are ingenious and clever, their drawbacks such as introduction of heavy metal ions or the use of tedious synthesis process blocks their practical application in clinical diagnosis. Therefore, development of a convenient fluorescence biosensor with better biocompatibility for serum ALP determination is urgently required.

Compared to the traditional fluorescence materials, such as fluorescent dyes, quantum dots, metal nanoclusters, etc., graphene quantum dots (GQDs), a novel kind of carbon-based nano fluorescent materials, have attracted considerable attention due to their benefits such as unique fluorescence properties, ease of production, low cytotoxicity and excellent biocompatibility [18–20]. These advantages have led to widespread GQDs use in biomedical fields, including the applications of constructing bionanocomposites, which is a promising strategy based on the construction of composites including biomolecules and nanomaterials [21,22]. The fascinatingly functional properties of GQDs have attracted particular attention in the fields of materials science and biological analysis [23]. By coupling nanomaterials with a diverse range of biomolecules, such as DNA [24], polypeptide [25], protein and biopolymers [26,27], researchers can combine the advantages of both components. Among these, chitosan (CS) is considered as one of the most promising components of bionanocomposites due to its unique physiochemical characteristics and biological activities [28]. The high contents of amino functional groups of CS make it positively charged under acidic or weak alkaline condition. This property is beneficial for the integration of CS with nano entities bearing negative charges by strong electrostatic interaction, and the adhesive behavior of CS is the basis of bionanocomposite formation [29]. Furthermore, its non-toxicity, biodegradability and antibacterial properties make it a desirable material for application in bioconjugation with nanomaterials in diverse applications such as electrochemical biosensing, bionanocomposites film formation, drug delivery and bioimaging [30–33].

In the current study, we designed a sodium hexametaphosphate ($(NaPO_3)_6$) modulated fluorescence responsive biosensor based on self-assembly/disassembly mode of reduced graphene quantum dots (rGQDs)/CS system for ALP (see Scheme 1). The rGQDs with bright blue emission and rich negative charged hydroxyl were prepared by chemically reducing GQDs with $NaBH_4$. The combination of rGQDs and CS via self-assembly offers a seminal breakthrough in the development of probes for ALP. The rGQDs act as both the fluorescent elements and the self-assembly building blocks. The CS charged biopolymer simultaneously exhibits both electrostatic attraction and structure transformation-induced fluorescence quenching of the rGQDs. Meanwhile, $(NaPO_3)_6$ which acts as the disassembly agent of the hybrid in this work also serves as the substrate of the phosphatase to enable its biological functions. When present, $(NaPO_3)_6$ competes with rGQDs for the binding sites on the CS, resulting in the disassembly of the combination between rGQDs and CS. Consequently, the rGQDs exhibit a turn-on PL signal. By introducing ALP into the system, $(NaPO_3)_6$ could be hydrolyzed to give phosphate anions, causing the influence of the disassembly agent on the rGQDs/CS system reduced by consuming part of the disassembly agent. So that the PL signal of rGQDs is decreased compared with the disassembly state of the rGQDs/CS system. The quenched PL intensity of GQDs is proportional to the concentration of ALP. The dynamic detection range for ALP is 20–500 mU mL^{-1}, which is much wider than most of the recently reported sensing platforms, and the detection limit (LOD) of 7.8 mU mL^{-1} is relatively low. Thus, an $(NaPO_3)_6$ modulated fluorescence responsive probe based on rGQDs/CS system for ALP was constructed. The present strategy shows high selectivity for ALP. When applied to real samples analysis, the method exhibits satisfactory results. In order to broaden its application, especially in the field of food safety detection, paper-based fluorescent sensors for ALP activity detection is urgently needed. These kind of sensors have potential for in situ fluorescent detection due to their simple fabrication, low cost, pocket friendly size and easy storage [34]. With the help of a hand-held ultraviolet lamp, the test strip can provide more intuitive detection results, making them more suitable for practical use. Herein, we immersed the filter paper in the rGQDs/CS solution to deposit the sensing hybrid on the filter paper, and then use the paper-based fluorescence test strips for ALP activity detection. The developed approach has good selectivity, low cost, is toxin-free and has a broad detection range. It also provides a new approach for the application of the hybrid system of GQDs and biopolymers.

2. Experiment

2.1. Reagents and materials

All of the chemicals used were of analytical reagent grade and required no further purification. Graphene powder, chitosan, $(NaPO_3)_6$, ATP, pyrophosphate (PPi), PO_4^{3-}, pyrophosphate (TTP) 2-Amino-2-(hydroxymethyl)-1,3-propanediol (Tris), $NaBH_4$, urea, reduced glutathione (GSH), glucose, ascorbic acid (AA), aspartic acid(Asp), glutamate (Glu), glycine (Gly), cysteine (Cys) and phenylalanine (Phe) were obtained from Beijing Dingguo Biotechnology Co. Ltd. ALP is acquired from TCI (Shanghai, China) Development Co. Ltd. and stored at −20 °C for cryopreservation. Deionized water with a resistivity higher than 18 MΩ cm^{-1} was used in the experiments. The stock solutions were diluted to the desired concentration with deionized water prior to use.

2.2. Apparatus

PL excitation and emission spectra are measured in a 1 cm path length quartz cuvette with a Shimadzu RF-5301 PC spectrofluorophotometer assembled with a Xenon lamp in the right-angle geometry. The morphology of rGQDs was observed with a JEOL-3010 electron microscope operating at 300 kV. Transmission electron microscopy (TEM) samples were prepared by dropping the aqueous rGQDs solution onto ultrathin films of carbon carbon-coated copper grids and allowing the excess solvent to evaporate in air. Atomic force microscopy (AFM) measurements were performed using a NanoScope Multimode AFM (Veeco, USA) using the tapping mode AFM. Dynamic Light Scattering (DLS) experiments were carried out with Malvern Instrument Zetasizer Nano ZS. UV–vis absorption spectra are obtained with a UV-2450 spectrophotometer (Shimadzu, Japan). FT-IR spectra were recorded with a Bruker IFS66V FT-IR spectrometer equipped with a DGTS detector (32 scans). All pH measurements were carried out with a Starter-2C pH meter obtained from Ohaus Instruments Co. Ltd., Shanghai, China. A ZF-5 portable three-use ultraviolet analyzer acquired from LOSON instrument Co. Ltd., Nanjing was used. All of the optical measurements were carried out at room temperature under ambient conditions.

2.3. Preparation and purification of rGQDs

GQDs were synthesized by cutting down graphene oxide (GO) through the hydrothermal approach as described in previous reports [35]. According to the reports in the literature [36], GO was prepared using graphite powder based on a modified Hummers' method. The resultant GO powder (0.05 g) was treated in concentrated H_2SO_4 (10 mL) and concentrated HNO_3 (3.3 mL). The mixture was subjected to ultrasonic treatment for 4 h and then transferred to a high-pressure reactor at 100 °C for 24 h. The mixture was naturally cooled to room temperature when the reaction was finished and was transferred into 130 mL of deionized water. The pH of the solution was adjusted to neutral by continuous addition of sodium bicarbonate. Dialysis was performed for 3 days to remove salt ions completely using a dialysis membrane (retained molecular weight: 1000 Da).

$NaBH_4$ can selectively reduce the carbonyl and epoxy moieties on the surface and edge of GQDs to hydroxyl groups in order to obtain rGQDs. Therefore, $NaBH_4$ (1 g) was added to the as-prepared GQDs solution (30 mL) and stirred for 4 h at room temperature. After the reduction, the product was transferred to a dialysis tube for complete elimination of the ions for 3 days. The final product solution was obtained with the concentration of 0.5 mg mL^{-1}.

2.4. Self-assemble and disassemble of rGQDs/CS bionanocomposites

The rGQDs fluorescent probe was prepared in a mixture (2 mL) containing 0.05 mg mL^{-1} rGQDs and 2.5 mM Tris-HCl (pH 7.4). Under the optimum incubation time and pH, the PL intensity of the rGQDs/CS bionanocomposites was assessed with continuous addition of CS from 5 to 1500 ng mL^{-1}.

The negatively charged rGQDs were captured by the positively charged CS through electrostatic assembly, giving rise to fluorescence quenching of rGQDs. When $(NaPO_3)_6$ is introduced into the self-assemble system, the disassemble process is triggered. To determine the appropriate concentration of $(NaPO_3)_6$ for use in the future $(NaPO_3)_6$-modulated rGQDs/CS system, the effects of $(NaPO_3)_6$ were studied. Solutions of Tris-HCl buffer (200 μL, 2.5 mM, pH 7.4), rGQDs (200 μL, 0.05 mg mL^{-1}), CS (10 μL, 1 μg mL^{-1}) were added sequentially to a centrifuge tube (2 mL) to incubate for 5 min. Then, various amounts of $(NaPO_3)_6$ solution were introduced to the above mixture. The PL intensity was recorded after persistent shaking for 25 min. The PL spectra were recorded in the emission wavelength range of 360–600 nm with the excitation at the wavelength of 310 nm.

2.5. Fluorescence detection for ALP activity

The determination of ALP activity was carried out by the enzymatic hydrolysis of $(NaPO_3)_6$ by ALP. The enzymatic reaction was performed by incubating mixtures with different concentrations of ALP and $(NaPO_3)_6$ solution for 3 h with constant shaking. Then the prepared rGQDs/CS sensing ensemble and the adequately reacted product mixture of the enzymatic reaction were successively added to a 2 mL calibrated test tube, brought to volume with deionized water and equilibrated for 25 min at room temperature. The final concentration of $(NaPO_3)_6$ in the tube was 5 μM and that of ALP ranged from 20 to 500 mU mL^{-1}. The PL spectra of the GQDs were recorded for wavelengths ranging from 360 nm to 600 nm and the PL intensity at the emission peak was used for the quantitative analysis of ALP under the optimized conditions. All of the measurements were repeated three times and the standard deviation was calculated for the error analysis.

2.6. Fetal calf serum samples detection

For practical biological samples detection, fetal calf serum (FCS) for commercial use was pretreated according to a previous report with a minor modification. To eliminate the interferences and improve the recovery, the FCS was split into several centrifuge tubes and centrifuged at 10,000 rpm for 10 min at room temperature. Equivoluminal acetonitrile (CH_3CN) was added to the separated supernatant of the FCS samples to precipitate the protein. After being well-mixed by fierce shaking, the mixture was centrifuged at 10,000 rpm for 10 min at 4 °C. The supernatant was filtered twice and adjusted to neutral pH with a buffer solution. Different concentrations of ALP were added to the 25 times diluted FSC samples to prepare the spiked samples. Real samples detection was carried out using the procedure described above.

3. Results and discussion

3.1. Characterization of rGQDs

The as-prepared GQDs were obtained from GO sheets through hydrothermal synthesis due to its simplicity and suitability for mass production. After purification, GQDs were then reduced to rGQDs by $NaBH_4$. The schematic diagram in Fig. S1 showed the preparation and purification process of rGQDs. The morphologies of rGQDs were characterized by TEM and AFM and are shown in Fig. 1a–c. The rGQDs in the images show good monodispersity, with a narrow lateral size distribution ranging from 2.0 to 4.4 nm and average particle sizes of 2.8 nm (shown in the size distribution histogram in Inset 2). The high-resolution TEM (HRTEM) image of rGQDs in Inset 1 showed an ordered crystal lattice, confirming that rGQDs are highly crystalline. The lattice spacing of 0.227 nm corresponds to the (1120) lattice fringes of graphene, which is in good agreement with the work of Li et al. [37]. Fig. 1b shows the AFM image of well-dispersed rGQDs. The height profile (Fig. 1c) reveals that the typical topographic height of the rGQDs are mainly distributed between 0.9 and 2.4 nm, implying that most of the rGQDs consist of 1–2 graphene layers. Compared to the original GQDs introduced in our previous work [38], these two kinds of GQDs have similarities in diameters and heights.

Then, FTIR measurements were carried out to verify the structure changes of GQDs and rGQDs. In Fig. 2a, both GQDs and rGQDs exhibit the stretching vibration bands of hydroxyl groups (-OH) that correspond to the absorption peaks at 3458 cm^{-1}. In addition, the bending vibration bands of –OH become stronger in the rGQDs spectra for the peaks at 1383 cm^{-1}. However, the vibration absorption bands of C═O (1635 cm^{-1}) and C–O–C (1117 cm^{-1} and 1206 cm^{-1}) become very weak in the rGQDs spectrum after $NaBH_4$ reduction. These results demonstrate that while the carbon skeleton of graphene is still present during the reduction progress, $NaBH_4$ can selectively reduce the carbonyl and epoxy moieties to hydroxyl groups. According to the research

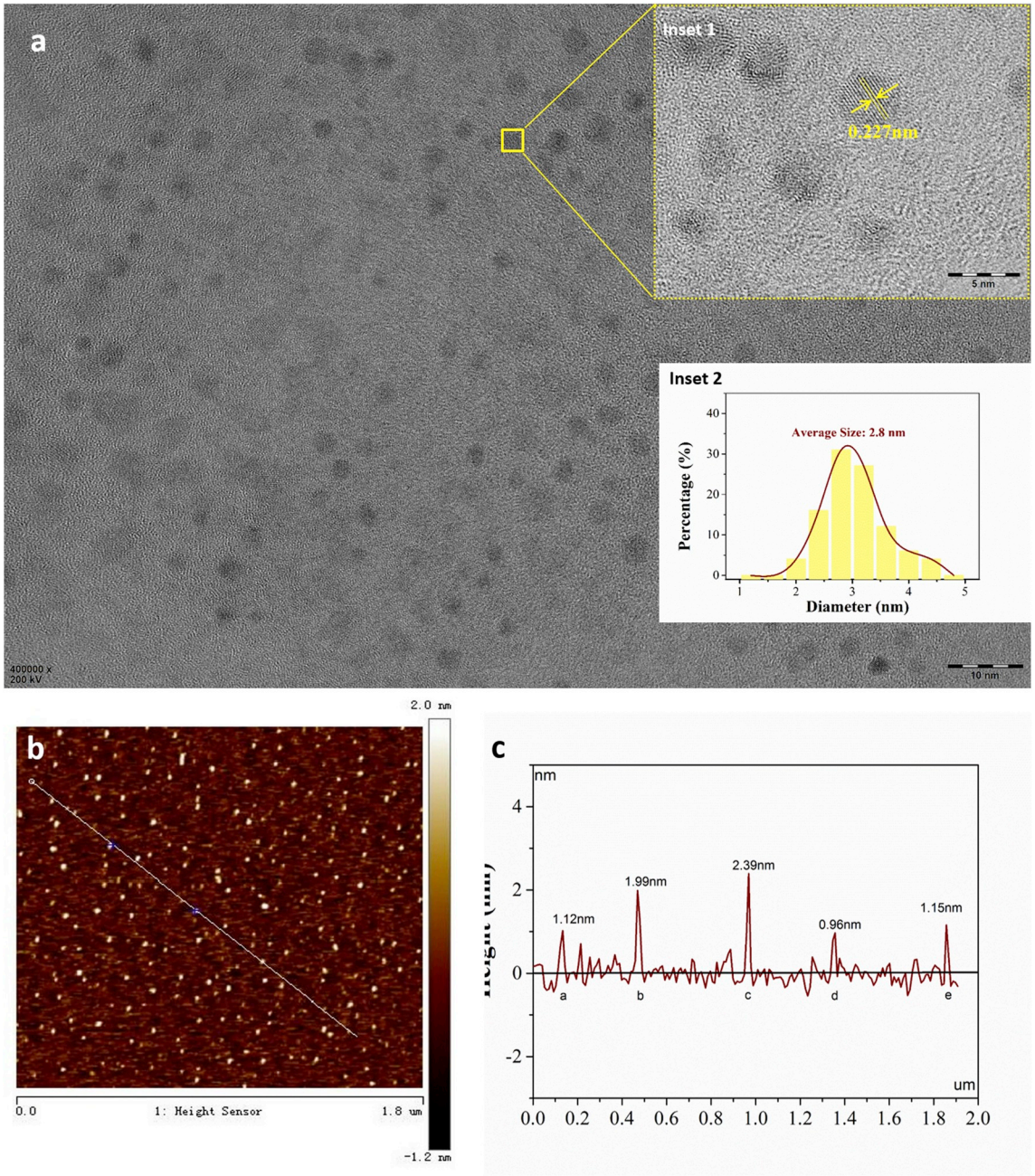

Fig. 1. (a) TEM images of rGQDs. The inset 1 of (a) is the HRTEM image of GQDs, the inset 2 of (a) is the size distributions of rGQDs; (b–c) The AFM image of GQDs and their corresponding topographic height profile analysis along the line shown in the image.

results reported by Zhu's group [37], the significantly increased amount of –OH groups on rGQDs makes the defect state emission of original GQDs transfer to the intrinsic state emission, suppressing the irradiative process. All of these changes make the blue emission play the leading role in rGQDs and enhance the fluorescence quantum yield. It is observed from Fig. 2b that compared to the weak PL intensity of the original GQDs, rGQDs result in a remarkably increased PL intensity that is approximately 1.5 times higher than that of GQDs and is accompanied with a significantly blueshifted emission peak (the peak position of rGQDs is at approximately 460 nm, which is 70 nm blueshifted from 530 nm of GQDs). The inset of Fig. 2c shows the photograph of the aqueous solutions of GQDs and rGQDs taken under irradiation by a 365 nm lamp. GQDs exhibit weak green fluorescence, while the rGQDs exhibit blue fluorescence with higher brightness. To further explore the optical properties of the GQDs, the UV–vis absorption and PL spectroscopy were studied. As illustrated in Fig. 2c, two absorption peaks are present in the UV–vis absorption spectrum of rGQDs: the peak ca. 230 nm is due to the π–π* transition of aromatic C–C bonds, and the shoulder ca. 310 nm is attributed to the n–π* transition of excited surface defects. However, unlike most fluorescent carbon nanoparticles, the as-prepared rGQDs display photoluminescence that is independent of the excitation wavelength change. As shown in Fig. 2d when the excitation wavelength varies from 280–370 nm, the PL peaks exhibit nearly no shift, whereas the PL intensity declines. The maximum emission intensity was obtained at 460 nm with the excitation wavelength of 310 nm. To consider the integrity of the spectral shape and the sensitivity of the assay, 310 nm was chosen as the excitation wavelength in the following study.

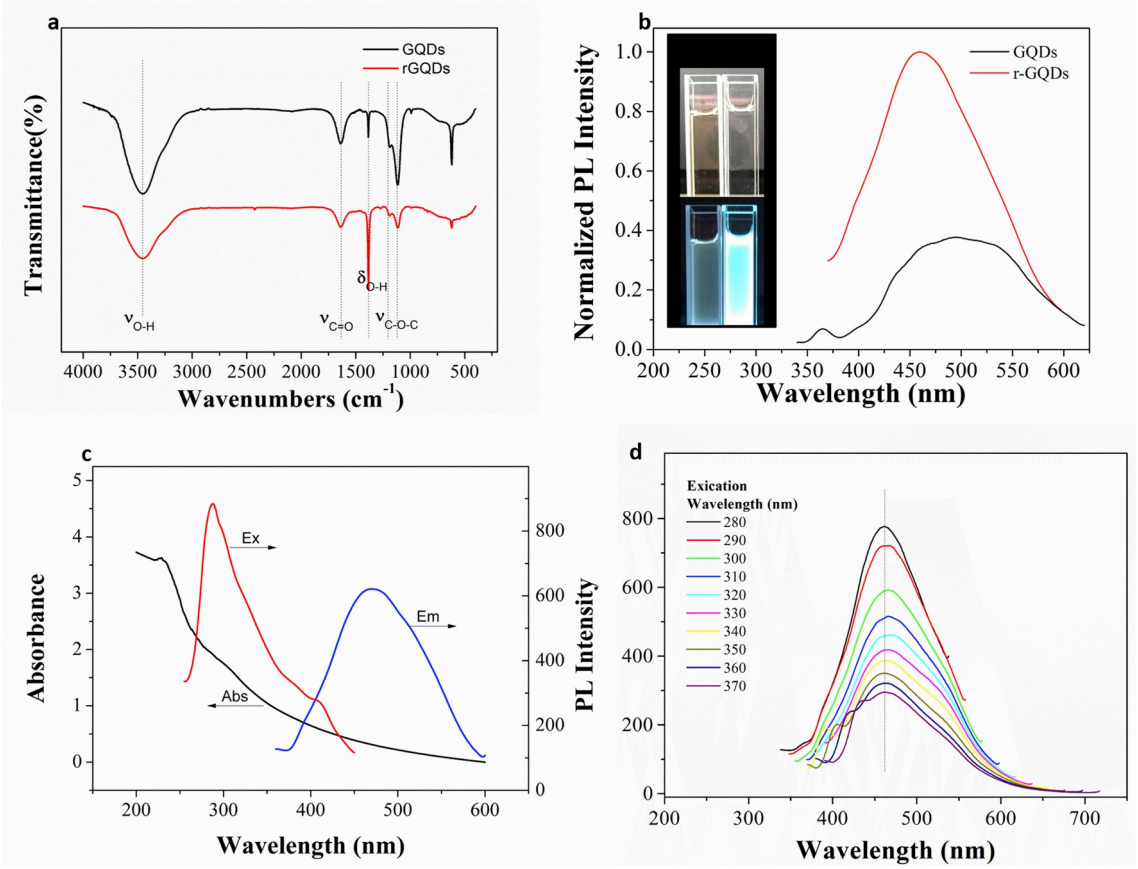

Fig. 2. (a) FT-IR spectra of as-prepared GQDs and rGQDs; (b) Normalized PL emission spectra of GQDs and rGQDs at the same concentration under 310 nm excitation wavelength. The inset of (e) is photographs of the GQDs (left) and rGQDs (right) solution taken under 365 nm UV light; (c) UV–Vis absorption, PL excitation and emission spectra of the rGQDs; (d) PL emission spectra of the rGQDs under different excitation wavelengths ranging from 280 nm to 370 nm. Experiments were performed at room temperature.

3.2. Self-assembly progress of rGQDs/CS biocomposites

The proof-of-concept experiment are performed to validate the feasibility of our sensing strategy. The histogram in Fig. 3 demonstrates the self-assembly/disassembly process after the rGQDs/CS system is mixed with $(NaPO_3)_6$ and $(NaPO_3)_6$-ALP hydrolysates, respectively. Since the electrostatic attraction and structure transformation-induced PL quenching of rGQDs, the addition of 1 μg mL^{-1} CS in to rGQDs solutions generates the rGQDs/CS system, causing the 2.8-fold increase of

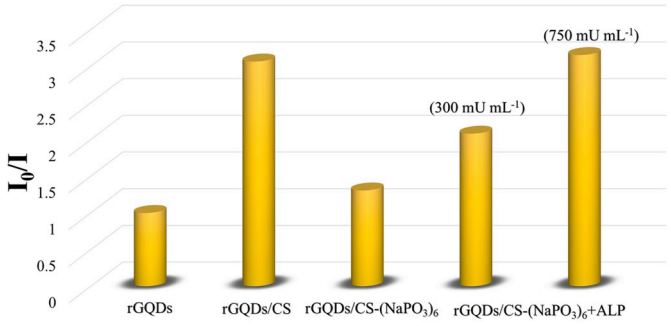

Fig. 3. The PL intensity ratio (I_0/I) of rGQDs, rGQDs/CS, rGQDs/CS-$(NaPO_3)_6$ system, and rGQDs/CS- $(NaPO_3)_6$ + ALP system in 5 mM Tris-HCl buffer (pH = 6.2). The concentration of rGQDs, CS, $(NaPO_3)_6$ and ALP were 50 μg mL^{-1}, 1 μg mL^{-1}, 5 μM, 300 mU $mL^{-1}$and 750 mU mL^{-1}, respectively.

the original value. Subsequently, the introduced 5 μM $(NaPO_3)_6$ disassembles the rGQDs/CS biocomposites by competing with rGQDs for the binding sites on the CS, displaying a remarkable reduction effect on the PL of rGQDs. When we incubate $(NaPO_3)_6$ with 300 mU mL^{-1}ALP first and then add the mixture to rGQDs/CS system, the quenched PL is observed again. This is due to the ALP-catalyzed conversion of $(NaPO_3)_6$ into phosphate ion that has a much weaker affinity to CS compared to rGQDs. Therefore, the biocomposites are barely disturbed.

To determine the optimal detection conditions, we systematically investigate the factors influencing the stability of the rGQDs/CS system and evaluate the quenching performance of CS for rGQDs. As mentioned above, electrostatic attraction is one of the main factors of the self-assembly reaction, and the status of the amino functional groups on CS determines the degree of its electronegativity. Therefore, the pH of the environment and ionic strength of solution are closely related to the self-assembly progress and affect the PL intensity of the rGQDs/CS system. The variation of PL intensity for rGQDs with different pH (6.2–9.0) values in the absence and presence of CS (1 μg mL^{-1}) was recorded and the results are shown in Fig. 4a. The PL intensity of rGQDs shows subtle changes with pH, whereas the rGQDs/CS system reveal intensive fluorescence suppression compared to the rGQDs alone for pH < 7.4. From the plotted data points shown in blue, it is observed that the quenching efficiency at acid or neutral environment is much higher than that under alkaline conditions. With an increase in the pH value, the quenching efficiency of CS decreased from 66.81% to 1.59%, demonstrating that alkaline conditions are not suitable for the stability of rGQDs/CS system. Additionally, the quenching performance is affected by increased ionic strength: the PL intensity of the rGQDs/CS

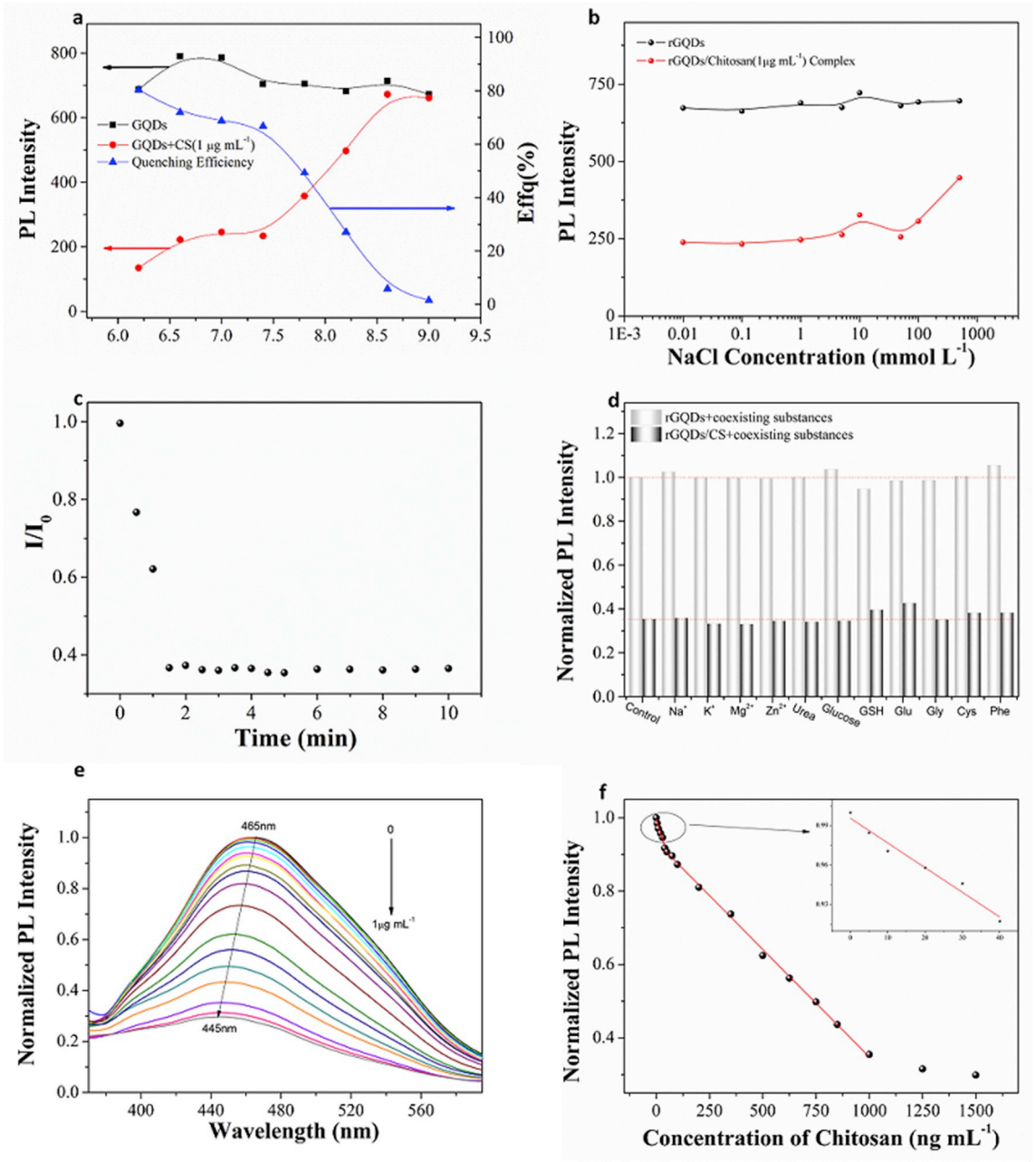

Fig. 4. (a) The effect of pH on the PL intensity of rGQDs in the absence(■) and presence (●) of CS (1 μg mL^{-1}) and the pH-dependent PL quenching efficiency (▲) of rGQDs by CS; (b) The effect of salt concentration(1 μM–1 M) on the PL intensity of rGQDs in the absence and presence of CS (1 μg mL^{-1}); (c) The temporal evolution on the PL intensity of rGQDs/CS system; (d) Interference resistibility of rGQDs/CS system over other coexisting substances (150 mM of Na^+, 5 mM of K^+, 1.5 mM of Mg^{2+}, 1 mM of Zn^{2+}, 3 mM of urea, 0.5 mM of GSH, 1 mM of glucose, 100 μM of Glu, Gly, Cys and Phe; (e) The PL emission spectra of rGQDs in the presence of different concentrations of CS (0–1 μg mL^{-1}); (f) The linear plot of normalized PL intensity versus CS concentrations in the range of 1–1500 ng mL^{-1}, inset is the linear plot of normalized PL intensity versus CS concentrations in the range of 1–40 ng mL^{-1}. All samples are prepared with Tris-HCl buffer solution (5 mM).

system shows insignificant changes when NaCl concentrations vary between 0 and 100 mM, implying that rGQDs do not aggregate within these ionic strength conditions, but increased gradually when the NaCl concentration was increased further to 1 M (Fig. 4b). Based on the above results, we conclude that low-pH and weak ionic strength environment can maximize the performance of the rGQDs/CS system, and electrostatic forces are vital for the self-assembly of the bionanocomposites. Considering the stability of the hybrid system and the optimal hydrolysis of ALP, pH 7.4 was chosen as the rGQDs/CS system working media. Fig. 4c illustrates the temporal evolution of the rGQDs/CS system. The self-assembly process requires only 2 min to reach equilibrium and the PL signal remained stable over the next 10 min. Therefore, we record the PL intensity after the rGQDs/CS system is incubated for 5 min. To test the resistance to interference of the rGQDs/CS system, the influences of other biologically relevant coexisting species containing metal ions (Na^+, K^+, Mg^{2+}, and Zn^{2+}), amino acids and small biological molecules to the system were investigated under the same conditions. As seen in Fig. 4d, rGQDs is not only insensitive to other potentially coexisting substances (light gray squares) but also respond well towards CS in the presence of these coexisting substances (dark gray squares). Therefore, the rGQDs/CS system is stable when sensing under physiological conditions.

The PL intensity evolution of rGQDs/CS system due to the different amounts of CS was investigated under the optimized conditions in order

to determine the suitable proportion of the bionanocomposites. The PL spectra of rGQDs coexisting with a series of CS concentrations were recorded and the results are displayed in Fig. 4e. Upon the increase in the CS concentration, the PL intensity of rGQDs was gradually decreased and the maximum emission wavelength of rGQDs was blueshifted from 460 nm to 445 nm. Fig. 4f shows that the plot of the normalized PL intensity versus the concentration of CS has good linearity in the range of 5–1000 ng mL^{-1}. The regression equations are:

$I/I_0 = (0.996 \pm 0.0348) + (-1.88 \times 10^{-3} \pm 1.55 \times 10^{-4})$ from 5 to 40 ng mL^{-1};

$I/I_0 = (0.935 \pm 0.0378) + (-5.87 \times 10^{-4} \pm 7.11 \times 10^{-6})$ from 40 to 1000 ng mL^{-1}

(I_0 and I are the PL intensities of rGQDs in the absence and presence of the CS, respectively). The correlation coefficients are $R^2 = 0.967$ and 0.998, with the detection limit (LOD) of 2.8 ng mL^{-1}. Finally, we choose 1 μg mL^{-1} CS to form the self-assembly system for further detection.

The quenching mechanism was studied in detail for purpose in order to investigate the high-efficiency self-assembly of the rGQDs/CS system. The PL spectra of the rGQDs/CS system exhibit an obvious blueshift of approximately 15 nm compared to that of rGQDs alone, indicating that the nature of the surface of the rGQDs has changed upon binding with CS. We speculate that the decrease of the molecular polarizability of the water of the self-assembled system and the intramolecular charge transfer between CS and rGQDs are responsible for the reductive Stokes shift [39]. Therefore, we investigate the TEM of the rGQDs and the rGQDs/CS self-assembling system to compare the morphology characteristics of rGQDs in the presence and absence of chitosan (Fig. S2). It is clear to see that, severe aggregation of rGQDs occurs in the presence of chitosan. This phenomenon proves that, there is a strong interaction between the two because of the electrostatic attraction. Then we use the dynamic light scattering (DLS) to study the particle size change of the electrostatic induced rGQDs/CS system. From Fig. S3, it can be seen that the diameter of rGQDs at the final CS concentration of 1 μg mL^{-1} changes from 28 nm to 141 nm, respectively. Therefore, the electrostatic attraction mentioned above may be the driving force in the formation of the self-assembly system. Based on this conclusion, we postulate that the predominant quenching mechanism is attributed to the energy transfer caused by the formation of quenched complexes. In other words, the quenching process may be static quenching. Static quenching can be confirmed through tiny changes in the UV–vis absorption spectra. The UV–vis absorption spectra of rGQDs, CS, rGQDs/CS system and rGQDs-CS mixture are shown in Fig. S4. Upon addition of CS, the absorption spectra of the rGQDs/CS system (curve c) do change in comparison with the data superposition (curve d) of the absorption spectra of the rGQDs (curve a) and CS (curve b), which is assigned to the complex formation of GQDs and CS, proving that static quenching indeed occurred.

3.3. Disassembly process of rGQDs/CS system by $(NaPO_3)_6$

We first investigate the effect of the reaction time on the disassembly of the rGQDs/CS system by $(NaPO_3)_6$. When the self-assembled process of the hybrid was stabilized, $(NaPO_3)_6$ with a concentration of 5 μM was added to the system. Its competitive binding to CS disassociates the bionanocomposites, leading to the rGQDs release into the aqueous solution and the recovery of the PL intensity of the mixture. Fig. 5a shows that the PL intensity of the $(NaPO_3)_6$-rGQDs/CS system gradually increases in the first 15 min and ultimately reaches equilibrium at approximately 10 min, and it is approximately 2.5 times stronger than the initial PL intensity. Thus, 25 min was chosen as the adequate reaction time for the further experiments.

Since the intense electronegativity of $(NaPO_3)_6$ is essential for the successful dissociation of the rGQDs/CS sensing ensemble, it is necessary to explore the tolerance of rGQDs/CS system to other negatively charged ions or biomolecules. We have recorded the variation in the PL intensity of this sensing system with 17 anions and small biomolecules under the same conditions, including PO_4^{3-}, PPi, ATP, TTP, HCO_3^-, $C_2O_4^{2-}$(Ac^-), NO_3^-, SO_4^{2-}, F^-, Cl^-, Br^-, I^-, S^{2-}, AA, Asp and Glu. The results in Fig. 5b indicate that no obvious disassembly of the rGQDs/CS system is observed in the presence of these common anions (dark gray bars). The interference experiments also clearly show that the coexistence of these anions has little influence on the $(NaPO_3)_6$-rGQDs/CS system (light gray bars). Therefore, $(NaPO_3)_6$ can be a superior disassembly agent for the rGQDs/CS system and the proposed sensing hybrid system is feasible for the subsequent ALP detection.

Next, quantitative detection of $(NaPO_3)_6$ based on the disassembly of rGQDs/CS system was performed. Fig. 5c describes a successive enhancement in the PL intensity of the rGQDs/CS system upon the gradual addition of $(NaPO_3)_6$ with the concentrations ranging from 0 to 20 μM. Meanwhile, the maximum emission wavelength of rGQDs was redshifted from 445 nm back to 461 nm again along with the recovery of the PL intensity, indicating the release of liberated rGQDs through the disassembly process. The calibration plot of the recovery efficiency $(I_r\text{-}I_q)/(I_0\text{-}I_q)$ as a function of $(NaPO_3)_6$ concentration is shown in Fig. 5d, in which I_0 and I_q are the PL intensities of rGQDs in the absence and presence of CS, respectively, and I_r is the PL intensity of the rGQDs/CS system in the presence of $(NaPO_3)_6$. The change in the PL intensity increases rapidly in the low concentration range of $(NaPO_3)_6$ (0–5 μM), and then increases slowly to a plateau when the $(NaPO_3)_6$ concentration increases up to 20 μM. Thus, $(NaPO_3)_6$ concentration of 5 μM for was determined as the fixed amount for the following quantitative measurement of ALP.

3.4. ALP assay based on the rGQDs/CS self-assembly system

ALP can specifically catalyze the hydrolysis and conversion of one $(NaPO_3)_6$ molecule into six phosphate ions under alkaline conditions, disturbing the disassembly of rGQDs/CS system and making rGQDs remain bound to CS. To improve the performance of the sensing system, the reaction temperature was optimized first. The effect of the hydrolysis temperature on the ALP activity for $(NaPO_3)_6$ is shown in Fig. 6a. The PL quenching effect of ALP on the rGQDs/CS-$(NaPO_3)_6$ system is promoted by increasing hydrolysis temperature and reaches maximum at 37 °C and then obviously decreases when the temperature exceeded 37 °C. This phenomenon is in accordance with the optimum temperature of the hydrolysis behavior of ALP. Therefore, we choose 37 °C as the optimal hydrolysis temperature for subsequent studies.

Under the optimized conditions, a fluorescence measurement of ALP activity was carried out. The changes in the PL intensity were recorded after the rGQDs/CS system was incubated with the reacted product mixtures with various concentrations of ALP and $(NaPO_3)_6$ for 20 min. The PL intensity of the rGQDs/CS-$(NaPO_3)_6$ system decreases gradually with increasing ALP concentration (from 20 to 500 mU mL^{-1}), and the maximum emission wavelength of the PL spectrum is once again blueshifted to 445 nm (Fig. 6b). Fig. 6c shows that a good linear relationship is observed between the PL intensity ratio of $(I_r\text{–}I)/(I_r\text{-}I_q)$ and ALP concentrations in the range of 20–500 mU mL^{-1}. The linear regression equation is:

$(I_r\text{–}I) / (I_r\text{-}I_q) = -0.01016 + 0.00194$, mU mL^{-1}

The corresponding regression coefficient is 0.995. The limit of detection (LOD) is 7.8 mU mL^{-1} using the criterion of three times the standard deviation of the blank signal. Since the obtained detection range of ALP can cover the normal level of serum ALP (40–190 mU mL^{-1} for adults) [40], the as-established probe is suitable for practical quantification of ALP levels with high accuracy in the serum of complex media and is also potentially useful for the diagnosis of the ALP-related diseases. In addition, we have compared the performance in the linear

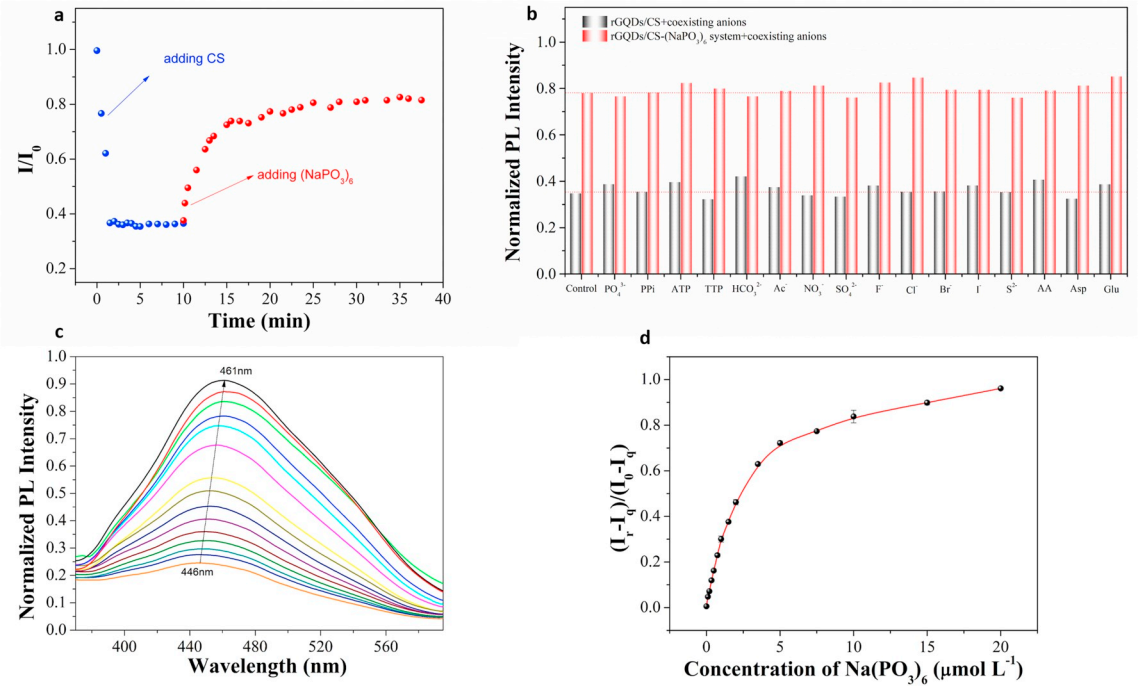

Fig. 5. (a) Time-dependent PL intensity of rGQDs upon addition of 1 μg mL^{-1} CS (blue dots) and 5 μM $(NaPO_3)_6$ after PL quenching by 1 μg mL^{-1} CS for 10 min (red dots); (b) Interference resistibility of rGQDs/CS-$(NaPO_3)_6$ system over other coexisting anions and small biological molecules, the concentration of $(NaPO_3)_6$ and other anions are all 5 μM; (c)The PL emission spectra of rGQDs/CS system in the presence of different concentrations of $(NaPO_3)_6$ (0–20 μM); (d) The plot of PL recovery efficiency$(I_r\text{-}I_q)/(I_0\text{-}I_q)$ of rGQDs/CS system versus $(NaPO_3)_6$ concentrations in the range of 1–20 μM (I_0 and I_q present the PL intensity of rGQDs in the absence and presence of CS, I_r presents the PL intensity of rGQDs/CS system in the presence of $(NaPO_3)_6$). All samples are prepared with Tris-HCl buffer solution (5 mM). (For interpretation of the references to color in this figure legend, the reader is referred to the Web version of this article.)

range and the LOD of the presented method to those for the other reported methods for ALP detection in Table S1. Our method offers a highly sensitive detection limit and a broader linear range across three orders of magnitude, which is either comparable or superior to those obtained from other sensitive systems.

3.5. Selectivity study

To assess the selectivity of the fluorescent assay for ALP, different enzymes and proteins such as trypsin, BSA, lysozyme, tyrosinase, thrombin, HSA and urease were investigated under parallel experimental conditions. Fig. 6d shows the quenching effect of the different enzymes on the rGQDs/CS-$(NaPO_3)_6$ system. The enzymes do not give rise to an obvious fluorescence quenching effect, so that only ALP gives a satisfactory response. The above results confirmed that the present assay system has high selectivity for ALP activity monitoring.

3.6. Test strips for ALP detection

By immobilization of the rGQDs/CS sensing ensemble on filter paper, test strips were constructed for ALP activity monitoring. As seen in Fig. 6e, the color change of the rGQDs/CS loaded test strips were observed with the naked eye upon exposure to UV irradiation. First, the test strip shows bright blue fluorescence color under UV illumination after 20 μL of $(NaPO_3)_6$ solution (5 μM) was dropped on the test strip for 40 min. With the increase in the ALP concentration in the test tube (0, 20, 50, … … and 750 mU mL^{-1}), the colors of the test papers gradually changed from the original blue to light blue, showing that the hydrolysis of ALP to $(NaPO_3)_6$ could strongly affect the bonding state of rGQDs and CS, enabling visual semi quantitation of the ALP activity.

3.7. Determination of ALP in fetal calf serum samples

To explore the feasibility of the presented ALP assay for use in complex biological samples, the sensing ensemble was used to detect spiked ALP in 50-fold fetal bovine serum (FBS) dilution and with the results listed in Table 1. The four ALP concentrations in the FBS samples were derived from the standard curve and the regression equation. The average recovery test was performed by applying the standard addition method. All of the data were collected from three independent measurements. The recovery range was between 97.42 and 102.58% and the RSD was lower than 4.28%. The above results have demonstrated the potential applicability of the rGQDs/CS system for the detection of ALP activity in biological samples.

4. Conclusion

To summarize, rGQDs with blue emission were prepared by chemically reducing GQDs with $NaBH_4$. The integration of rGQDs and CS via self-assembly/disassembly offers an excellent design of a label-free probe for ALP. Taking advantage of the modulation of $(NaPO_3)_6$ to the rGQDs/CS system and the hydrolysis of ALP to $(NaPO_3)_6$, we successfully constructed a “turn-on-off” sensing mode for ALP assay, with the LOD as low as 7.8 mU mL^{-1}, and the detection range that is wide enough to cover the normal concentration level of serum ALP. The developed approach displays good selectivity for ALP and exhibits satisfactory results when applied to real samples analysis. This low-cost, toxin-free probe provides a new approach for the biosensing applications of the hybrid system of GQDs and biopolymers.

Acknowledgments

We truly appreciate the financial support from the National Natural Science Foundation of China, China (21775052), the Taishan Scholar Program of Shandong Province (No. ts 201511027) and Qingdao postdoctoral research project funding.

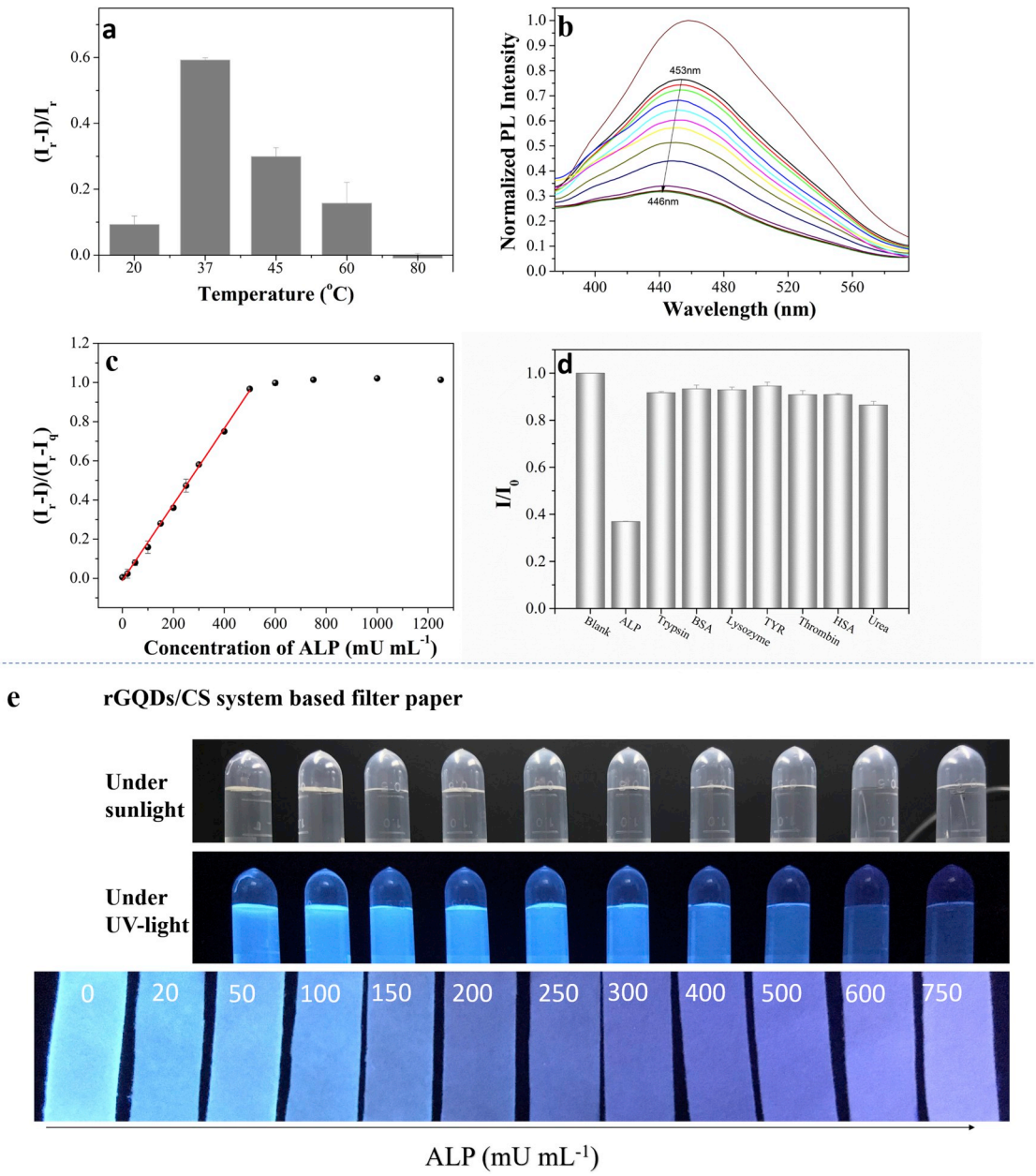

Fig. 6. (a) Effect of incubation temperature on the PL intensity ratio $(I_r–I)/I_r$ of ALP to the rGQDs/CS-$(NaPO_3)_6$ system, I_r and I present the PL intensity of rGQDs/CS-$(NaPO_3)_6$ system in the absence and presence of ALP; (b) The PL emission spectra of rGQDs/CS-$(NaPO_3)_6$ system in the presence of different concentrations of ALP (0–1.2 U mL^{-1}); (c) The linear plot of quenching efficiency$(I_r–I)/(I_r-I_q)$ of rGQDs/CS-$(NaPO_3)_6$ system versus ALP concentrations in the range of 20–500 mU mL^{-1} (I_q and I_r present the PL intensity of rGQDs/CS system in the absence and presence of $(NaPO_3)_6$, I presents the PL intensity of rGQDs/CS-$(NaPO_3)_6$ system in the presence of ALP; (d) Quenching effect of the rGQDs/CS-$(NaPO_3)_6$ system in the presence of 500 mU mL^{-1} trypsin (0.1 ng mL^{-1} or 1.85 nM) and other enzymes (1 μg mL^{-1} for trypsin, 4 mg mL^{-1} for BSA and HSA, 10 μg mL^{-1} for lysozyme, 1 mg mL^{-1} for tyrosinase and 10 μM for thrombin and urease) at 37 °C. All samples are prepared with Tris-HCl buffer solution (5 mM); (e) Photographs of the rGQDs/CS solutions upon the addition of certain amount of $(NaPO_3)_6$ with different concentrations of ALP: 0, 20, 50, 100, 150, 200, 250, 300, 400, 500, 600, 750 mU mL^{-1} under sunlight and UV (365 nm) illumination and the corresponding photograph of rGQDs/CS system based filter paper strips under UV illumination (365 nm). Conditions in (e): Tris-HCl buffer solution (5 mM), CS (1 μg mL^{-1}) and $(NaPO_3)_6$(5 μM).

Table 1
Measurements of ALP in fetal calf serum samples using the proposed probe. *

Added (mU mL^{-1})	Found (mU mL^{-1})	RSD (n = 3, %)	Recovery (%)
50	51.29	3.71	102.58
100	97.42	4.28	97.42
250	247.15	1.85	98.86
400	399.58	1.69	99.89

*The original concentrations of ALP in fetal calf serum sampssles were subjected to a 50-fold dilution with Tris-HCl buffer before detection. (Tris-HCl, 0.1 M, pH = 7.4).

Appendix A. Supplementary data

Supplementary data to this article can be found online at https://doi.org/10.1016/j.talanta.2019.120341.

References

[1] D.J. Goldstein, C.E. Rogers, H. Harris, Expression of alkaline phosphatase loci in mammalian tissues, Proc. Natl. Acad. Sci. 77 (1980) 2857–2860.
[2] P. Schrenkhammer, I.C. Rosnizeck, A. Duerkop, O.S. Wolfbeis, M. Schäferling, Time-resolved fluorescence-based assay for the determination of alkaline phosphatase activity and application to the screening of its inhibitors, J. Biomol. Screen

13 (2007) 9–16.
[3] R.E. Gyurcsanyi, A. Bereczki, G. Nagy, M.R. Neuman, E. Lindner, Amperometric microcells for alkaline phosphatase assay, Analyst 127 (2002) 235–240.
[4] K. Ooi, K. Shiraki, Y. Morishita, T. Nobori, High-molecular intestinal alkaline phosphatase in chronic liver diseases, J. Clin. Lab. Anal. 21 (2007) 133–139.
[5] P.L. Wolf, Clinical significance of serum high-molecular-mass alkaline phosphatase, alkaline phosphatase–lipoprotein-X complex, and intestinal variant alkaline phosphatase, J. Clin. Lab. Anal. 8 (1994) 172–176.
[6] A. Andersson, L. BrattstrÖM, B. Israelsson, A. Isaksson, A. Hamfelt, B. Hultberg, Plasma homocysteine before and after methionine loading with regard to age, gender, and menopausal status, Eur. J. Clin. Investig. 22 (1992) 79–87.
[7] L. Jia, J.-P. Xu, D. Li, S.-P. Pang, Y. Fang, Z.-G. Song, J. Ji, Fluorescence detection of alkaline phosphatase activity with [small beta]-cyclodextrin-modified quantum dots, Chem. Commun. 46 (2010) 7166–7168.
[8] J. Liu, D. Tang, Z. Chen, X. Yan, Z. Zhong, L. Kang, J. Yao, Chemical redox modulated fluorescence of nitrogen-doped graphene quantum dots for probing the activity of alkaline phosphatase, Biosens. Bioelectron. 94 (2017) 271–277.
[9] Z. Qian, L. Chai, C. Tang, Y. Huang, J. Chen, H. Feng, Carbon quantum dots-based recyclable real-time fluorescence assay for alkaline phosphatase with adenosine triphosphate as substrate, Anal. Chem. 87 (2015) 2966–2973.
[10] Z.S. Qian, L.J. Chai, Y.Y. Huang, C. Tang, J. Jia Shen, J.R. Chen, H. Feng, A real-time fluorescent assay for the detection of alkaline phosphatase activity based on carbon quantum dots, Biosens. Bioelectron. 68 (2015) 675–680.
[11] C. Tang, Z. Qian, Y. Huang, J. Xu, H. Ao, M. Zhao, J. Zhou, J. Chen, H. Feng, A fluorometric assay for alkaline phosphatase activity based on β-cyclodextrin-modified carbon quantum dots through host-guest recognition, Biosens. Bioelectron. 83 (2016) 274–280.
[12] M.-H. Xiang, J.-W. Liu, N. Li, H. Tang, R.-Q. Yu, J.-H. Jiang, A fluorescent graphitic carbon nitride nanosheet biosensor for highly sensitive, label-free detection of alkaline phosphatase, Nanoscale 8 (2016) 4727–4732.
[13] Y. Zhu, G. Wang, H. Jiang, L. Chen, X. Zhang, One-step ultrasonic synthesis of graphene quantum dots with high quantum yield and their application in sensing alkaline phosphatase, Chem. Commun. 51 (2015) 948–951.
[14] S. Liu, X. Wang, S. Pang, W. Na, X. Yan, X. Su, Fluorescence detection of adenosine-5′-triphosphate and alkaline phosphatase based on the generation of CdS quantum dots, Anal. Chim. Acta 827 (2014) 103–110.
[15] J. Liang, R.T.K. Kwok, H. Shi, B.Z. Tang, B. Liu, Fluorescent light-up probe with aggregation-induced emission characteristics for alkaline phosphatase sensing and activity study, ACS Appl. Mater. Interfaces 5 (2013) 8784–8789.
[16] Z. Song, Y. Hong, R.T.K. Kwok, J.W.Y. Lam, B. Liu, B.Z. Tang, A dual-mode fluorescence “turn-on” biosensor based on an aggregation-induced emission luminogen, J. Mater. Chem. B. 2 (2014) 1717–1723.
[17] F. Zheng, S. Guo, F. Zeng, J. Li, S. Wu, Ratiometric fluorescent probe for alkaline phosphatase based on betaine-modified polyethylenimine via excimer/monomer conversion, Anal. Chem. 86 (2014) 9873–9879.
[18] V. Georgakilas, M. Otyepka, A.B. Bourlinos, V. Chandra, N. Kim, K.C. Kemp, P. Hobza, R. Zboril, K.S. Kim, Functionalization of graphene: covalent and non-covalent approaches, derivatives and applications, Chem. Rev. 112 (2012) 6156–6214.
[19] J. Shen, Y. Zhu, X. Yang, C. Li, Graphene quantum dots: emergent nanolights for bioimaging, sensors, catalysis and photovoltaic devices, Chem. Commun. 48 (2012) 3686–3699.
[20] J. Yao, Y. Sun, M. Yang, Y. Duan, Chemistry, physics and biology of graphene-based nanomaterials: new horizons for sensing, imaging and medicine, J. Mater. Chem. 22 (2012) 14313–14329.
[21] H. Razmi, V. Abdollahi, R. Mohammad-Rezaei, Graphene quantum dots–eggshell nanocomposite to extract polycyclic aromatic hydrocarbons in water, Environ. Chem. Lett. 14 (2016) 521–526.
[22] F.-F. Zheng, P.-H. Zhang, Y. Xi, J.-J. Chen, L.-L. Li, J.-J. Zhu, Aptamer/graphene quantum dots nanocomposite capped fluorescent mesoporous silica nanoparticles for intracellular drug delivery and real-time monitoring of drug release, Anal. Chem. 87 (2015) 11739–11745.
[23] H.B. Yao, Z.H. Tan, H.Y. Fang, S.H. Yu, Artificial nacre-like bionanocomposite films from the self-assembly of chitosan-montmorillonite hybrid building blocks, Angew. Chem. Int. Ed. 49 (2010) 10127–10131.
[24] C.A. Mirkin, Programming the assembly of two- and three-dimensional architectures with DNA and nanoscale inorganic building blocks, Inorg. Chem. 39 (2000) 2258–2272.
[25] J. Li, Q. Han, X. Wang, N. Yu, L. Yang, R. Yang, C. Wang, Reduced aggregation and cytotoxicity of amyloid peptides by graphene oxide/gold nanocomposites prepared by pulsed laser ablation in water, Small 10 (2014) 4386–4394.
[26] Y. Lin, R. Chapman, M.M. Stevens, Integrative self-assembly of graphene quantum dots and biopolymers into a versatile biosensing toolkit, Adv. Funct. Mater. 25 (2015) 3183–3192.
[27] T. Yang, Z. Li, L. Wang, C. Guo, Y. Sun, Synthesis, characterization, and self-assembly of protein lysozyme monolayer-stabilized gold nanoparticles, Langmuir 23 (2007) 10533–10538.
[28] S. Sarin, S. Kolesnikova, I. Postnova, C.-S. Ha, Y. Shchipunov, Bionanocomposite from self-assembled building blocks of nacre-like crystalline polymorph of chitosan with clay nanoplatelets, RSC Adv. 6 (2016) 33501–33509.
[29] G.L. Martin, J.A. Ross, S.D. Minteer, D.M. Jameson, M.J. Cooney, Fluorescence characterization of chemical microenvironments in hydrophobically modified chitosan, Carbohydr. Polym. 77 (2009) 695–702.
[30] Q. Meng, W. Su, C. He, C. Duan, Novel chitosan-based fluorescent materials for the selective detection and adsorption of Fe^{3+} in water and consequent bio-imaging applications, Talanta 97 (2012) 456–461.
[31] N. Butwong, L. Zhou, E. Moore, S. Srijaranai, J.H.T. Luong, J.D. Glennon, A highly sensitive hydrogen peroxide biosensor based on hemoglobin immobilized on cadmium sulfide quantum dots/chitosan composite modified glassy carbon electrode, Electroanalysis 26 (2014) 2465–2473.
[32] Y. Guo, X. Ge, J. Guan, L. Wu, F. Zhao, H. Li, X. Mu, Y. Jiang, A. Chen, A novel method for fabricating hybrid biobased nanocomposites film with stable fluorescence containing CdTe quantum dots and montmorillonite-chitosan nanosheets, Carbohydr. Polym. 145 (2016) 13–19.
[33] O. Lv, Y. Tao, Y. Qin, C. Chen, Y. Pan, L. Deng, L. Liu, Y. Kong, Materials for biological applications,Highly fluorescent and morphology-controllable graphene quantum dots-chitosan hybrid xerogels for in vivo imaging and pH-sensitive drug carrier, Mater. Sci. Eng. C 67 (2016) 478–485.
[34] D.M. Cate, J.A. Adkins, J. Mettakoonpitak, C.S. Henry, Recent developments in paper-based microfluidic devices, Anal. Chem. 87 (2015) 19–41.
[35] D. Pan, J. Zhang, Z. Li, M. Wu, Hydrothermal route for cutting graphene sheets into blue-luminescent graphene quantum dots, Adv. Mater. 22 (2010) 734–738.
[36] Y. Gao, Y. Li, L. Zhang, H. Huang, J. Hu, S.M. Shah, X. Su, Adsorption and removal of tetracycline antibiotics from aqueous solution by graphene oxide, J. Colloid Interface Sci. 368 (2012) 540–546.
[37] S. Zhu, J. Zhang, S. Tang, C. Qiao, L. Wang, H. Wang, X. Liu, B. Li, Y. Li, W. Yu, X. Wang, H. Sun, B. Yang, Surface chemistry routes to modulate the photoluminescence of graphene quantum dots: from fluorescence mechanism to up-conversion bioimaging applications, Adv. Funct. Mater. T22 (2012) 4732–4740.
[38] F. Shi, Y. Zhang, W. Na, X. Zhang, Y. Li, X. Su, Graphene quantum dots as selective fluorescence sensor for the detection of ascorbic acid and acid phosphatase via Cr(vi)/Cr(iii)-modulated redox reaction, J. Mater. Chem. B 4 (2016) 3278–3285.
[39] H. Wang, C. Zheng, T. Dong, K. Liu, H. Han, J. Liang, Wavelength dependence of fluorescence quenching of CdTe quantum dots by gold nanoclusters, J. Phys. Chem. C 117 (2013) 3011–3018.
[40] T.U. Hausamen, R. Helger, W. Rick, W. Gross, Optimal conditions for the determination of serum alkaline phosphatase by a new kinetic method, Clin. Chim. Acta 15 (1967) 241–245.